Proceedings of ASME Turbo Expo 2011
GT2011
June 6-10, 2011, Vancouver, British Columbia, Canada

GT2011-46050

A Simplified CFD Model with Multi-Periodic Boundary Conditions for Cross Wavy Channels

L. X. Du, M. Zeng and Q. W. Wang*

Key Laboratory of Thermal Fluid Science and Engineering of MOE
Xi'an Jiaotong University, Xi'an, Shaanxi, 710049, P.R. China

ABSTRACT

The compact and efficient primary surface heat exchangers are often used as recuperators in microturbine regenerative cycle systems. In the present study, the flow and the heat transfer performance of the cross wavy (CW) ducts have been simulated by three-dimensional models. The hydrodynamic diameters of the models are 1.689mm. Navier-Stokes and energy equations are solved by COMSOL3.5. Because one single wavy cell will overlap more than one adjacent channel, multi-periodic boundary conditions are especially adopted to simplify the calculations. Multi-periodic boundary conditions have been proved to have more reasonable flow field and heat transfer coefficient compared with the literature results. A dimensionless parameter L/A (wave length L, internal height of the corrugation in flow direction A) is defined as the optimization target. The numerical results indicated that when $L/A = 6$, the CW channel has the best comprehensive performance in all the cases. The comprehensive performances of the CW ducts are evaluated by the j/f (heat transfer factor j and friction factor f). The flow and heat transfer characteristics are much more complex in the cross wavy channels, especially when L/A is small. [**Keywords:** recuperator; cross wavy; multi-periodic boundary conditions]

INTRODUCTION

For the problems of exhausting of energy resources and the deteriorating of environment, microturbines have been proved to be particularly attractive for the power generation market especially in the Disturbed Power Generation System (DGS). The main advantages of the microturbines are smaller size and weight, lower emissions and noise, fuel flexibility and reduced maintenance. Microturnines based the proven technology can approach a thermal efficiency of 30% or higher with a compact primary surface recuperator [1-4]. Present manufacturing techniques provide the means of designing very compact recuperator cores and overcoming the disadvantages of the former recuperators which are bulky size, poor reliability and high cost. By the limitation of the metal material, the method of increasing the inlet temperature and pressure ratio to improve the cycle efficiency is limited [4]. The primary surface recuperators which are light weight, low pressure loss, high heat-transfer coefficient, small volume and high reliability, are suitable to be used in the regenerative cycles. In the past three decades, researchers have been attracted in designing the recuperator cores and the primary surface sheets.

The annular wrap-around recuperators and split type rectangular recuperators have been used in the regenerative cycle [3-4]. The patterns of the primary surface sheet have different types of Cross-Wavy (CW), Cross-Corrugated (CC), Cross-Undulated (CU) and so on [5]. Rekuperator Svenska AB company [6] has successfully developed a completely laser welded recuperator which the thermal performance is very competitive for a 100 kW microturbine applications [7]. McDonald [3-4] had discussed the Recuperator considerations for future higher efficiency microturbines and Low-cost compact primary surface recuperator concept for microturbines.

The numerical and experimental investigations of the compact primary surface recuperator have been done by many relevant researchers. Usually, it is expensive to manufacture a prototype recuperator and test its performance during design stage, so the researchers use CFD (Computational Fluid Dynamics) and NHT (Numerical Heat Transfer) methods to investigate the heat transfer behaviors in the recuperator core region and predict the flow characteristic in the primary surface sheets flow channels.

The existing literatures have done a lot of numerical investigations and experimental studies on different patterns of the primary surface sheets [8-14]. Utriainen & Suden [9] have numerically investigated the flow and heat transfer behavior in the CW unit cell by a simplified model (as shown in Fig. 1). Partial periodic boundary conditions were adopted in the main flow direction by adding extra source terms in the momentum and temperature equations and fully periodic boundary conditions are applied in the passages between adjacent channels perpendicular to the main flow direction.

For in the former literatures, very few researchers use simplified models with multi-periodic boundary conditions, and also very little attention has been focused on the models as shown in Fig.2. When the amplitude of the duct in the flow direction becomes bigger, there is a gap in the CW channels. In this case the flow becomes much more complex and the local heat transfer coefficient is enhanced. In our present work, several simplified models (as shown in Fig. 2) have been established, and multi-periodic boundary conditions have been used in the numerical investigations. The performances of different CW channels have been numerically studied by COMSOL3.5.

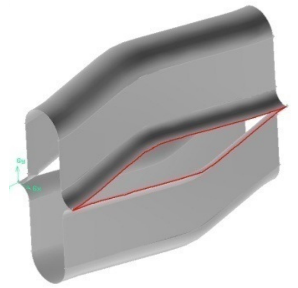

Figure 1 One case of the CW flow passages

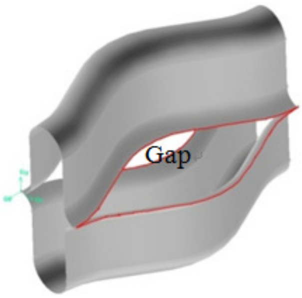

Figure 2 Another case of the CW flow passages

NOMENCLATURE

L	The length of the unit cell[mm]
A	The amplitude of the unit cell[mm]
T(x,y,z)	The temperature in the surface[K]
$T_b(z)$	The average temperature in z-surface[K]
T_w	The wall temperature[K]
T_{ave}	The average temperature of the surface[K]
x,y,z	Coordinate directions [m]
u_m	The average velocity magnitude[m/s]
u,v,w	Coordinate velocities[m/s]
Re	Reynolds number
Nu	Nusselt number
Pr	Prandtl number
St	Stanton number
d_e	Hydraulic diameter[mm]
k_{dv}	Dilatational viscosity[$\mathrm{Pa \cdot s}$]
h	Convective heat-transfer coefficient[$\mathrm{W/(m^2 \cdot K)}$]
$\mathbf{u}$	Velocity[m/s]
$\mathbf{F}$	Volume force[$\mathrm{N/m^3}$]
$\mathbf{I}$	Unit vector
η	Dynamic viscosity[$\mathrm{Pa \cdot s}$]
ρ	Density[$\mathrm{kg/m^3}$]
f	Friction factor
j	Heat transfer factor

MATHEMATICAL MODELS AND GOVERNING EQUATIONS

As shown in Fig. 3, the air cell of CW heat exchanger has two primary surface sheets and the channels of the upper and lower sheets have a phase angle of 180^0. We can find that the recuperator core can be simplified to a unit cell as shown in Fig. 4, and the simplified model can be used to solve the fully developed flow characteristic and heat transfer performance in the CW passages. Figure 4 also shows the main geometrical variables of the unit cell L (the length of the cell), A (the amplitude of the cell in the main flow direction), H (the height of the cell) and P (the width of the cell in the section direction).

In Table 1, the geometrical variables of the models used in the computation have been given. The optimization target of the study is the geometrical variables of the cell in the flow direction, so in all cases we just change the variables of L and A. The range of L/A is from 3.0 to 10.0 in the present study. For the simplified models have periodicities in the main flow direction and the direction perpendicular to the main flow direction, multi-periodic boundary conditions have been used in the numerical investigations.

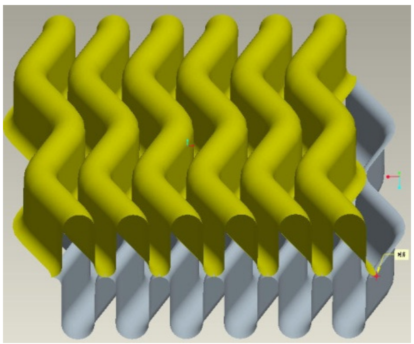

Fig. 3 CW surface sheets stack

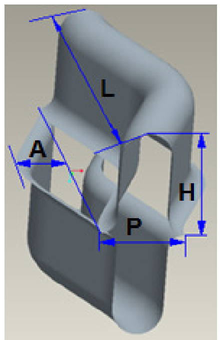

Fig. 4 CW unit cell

Figure 5 contains one upper duct and four lower channels, and the gap between two adjacent channels will increase as the increasing of the amplitude of the cell. It means that the duct will open up the passages to more adjacent passages, thus larger scale secondary flows are created and the flow maldistribution, reflux in the passages will be much more serious. As shown in Fig.5, the faying surfaces are separated into eight parts, and four fully periodic boundary conditions have been used (the relationship between corresponding parts are F1 and F1', F2 and F2', F3 and F3', F4 and F4'). Comparing with the models used by other researchers [9], there are gaps between adjacent channels and faying surfaces have been separated into different parts to utilize fully periodic boundary conditions.

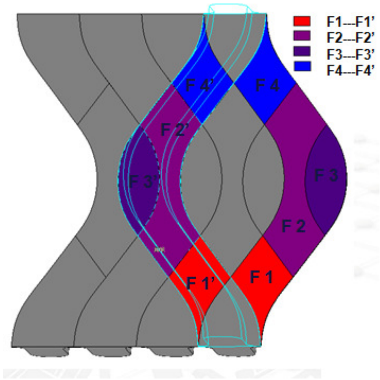

Fig. 5 Numerical models

Table1 Geometrical variables of the models

Channels	*L* (mm)	*A* (mm)	*P* (mm)	*H* (mm)	d_e (mm)
CWL6.4A1.6	6.4	1.6	1.8	2.2	1.689
CWL9.6A0.96	9.6	0.96	1.8	2.2	1.689
CWL9.6A1.2	9.6	1.2	1.8	2.2	1.689
CWL9.6A1.6	9.6	1.6	1.8	2.2	1.689
CWL9.6A2.4	9.6	2.4	1.8	2.2	1.689
CWL9.6A3.2	9.6	3.2	1.8	2.2	1.689

In the computations, periodic boundary conditions have been used in the main flow direction and the faying surfaces. The walls are set as constant temperature boundary conditions. Incompressible and constant properties of the fluid are assumed. For the Reynolds number considered in this study ranges from 100 to 1000, and a laminar flow is assumed in all computations.

The following equations are valid for these cases:

The continuity equation:

$$\nabla \mathbf{u} = 0 \tag{1}$$

The Navier-Stokes equation:

$$\rho(\mathbf{u}\cdot\nabla)\mathbf{u} = \nabla\cdot[-P\mathbf{I} + \eta(\nabla\mathbf{u} + (\nabla\mathbf{u})^T) - (2\eta/3 - k_{dv})(\nabla\cdot\mathbf{u})\mathbf{I}] + \mathbf{F} \tag{2}$$

The energy equation:

$$\nabla\cdot(k\cdot\nabla T) = Q - \rho C_p \mathbf{u}\cdot\nabla T \tag{3}$$

where T is the temperature, **u** is the velocity field.

In the flow direction:

The velocity equation:

$$\begin{Bmatrix} u_{in}(x,y,z) = u_{out}(x,y,z+L) \\ v_{in}(x,y,z) = v_{out}(x,y,z+L) \\ w_{in}(x,y,z) = w_{out}(x,y,z+L) \end{Bmatrix} \tag{4}$$

The temperature equation:

$$\frac{T_{in}(x,y,z) - T_w}{T_b(z) - T_w} = \frac{T_{out}(x,y,z+L) - T_w}{T_b(z+L) - T_w} \tag{5}$$

where u, v and w are the velocity components in cartesian coordinate system, T_{in}(x,y,z) and T_{out}(x,y,z+L) are the temperatures in the inlet and outlet surfaces, T_b(z) and T_b(z+L) are the average temperatures of the inlet and the outlet surfaces[15]. The average temperature of the surface is calculated by equation (8).

In the computation, an initial flow field has been got by using velocity inlet boundary conditions, and the inlet pressure of the cell are calculated by the internal pressure equations of COMSOL3.5 which are controlled by the mass flow rate. Then the periodic boundary condition is added in the main flow direction and the inlet pressure calculated is used as the initial pressure field of the inlet.

In the faying surfaces:

The velocity equation:

$$\begin{Bmatrix} u_{F_i} = u_{F_i'} \\ v_{F_i} = v_{F_i'} \\ w_{F_i} = w_{F_i'} \end{Bmatrix} \qquad (i = 1,2,3,4) \tag{6}$$

The temperature equation:

$$T_{F_i} = T_{F_i'} \qquad (i = 1,\ 2,\ 3,\ 4) \tag{7}$$

where T_{F_i} and $T_{F_i'}$ are the temperature in the faying surfaces[15].

The average temperature of the surface:

$$T_{ave} = \frac{\int_A u_m T dA}{A u_m} \tag{8}$$

The fanning friction factor:

$$f = \frac{\Delta P d_e}{\rho L u_m^2 / 2} \tag{9}$$

The heat transfer factor:

$$\mathrm{j} = St \cdot Pr^{2/3}$$

$$St = \frac{h}{\rho u_m C_P} \tag{10}$$

where Pr is the Prandtl number and St is the Stanton number.

GRID INDEPENDENCE AND MODEL VALIDATION

From Fig. 6, it can be found that the pressure loss has a little difference (the biggest difference is about 1%) between different cells number, and it indicates that the grid cells used in the computations have little effects on the numerical results. The number of degrees of freedom in the third case is 194,740. To ensure the independency of the grid system, the last case is used.

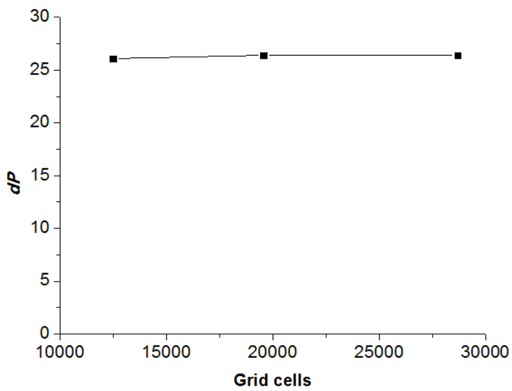

Fig. 6 Grid independence

The flow and heat transfer characteristics in the infinitely narrow crack have been simulated and the velocity field is shown in Fig.7. Please note that, double periodic boundary conditions (used in the main flow direction and in one pair of the side surfaces) have been used in the computation. In this case, the computational Nusselt number is 7.686 and the theoretical analytical Nusselt number is 7.54, the difference between the computation and the theoretical Nusselt numbers is about 2%. So it is acceptable to use multi-periodic boundary conditions to solve the flow and heat transfer characteristics in the CW unit cell.

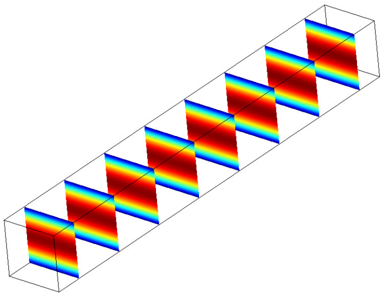

Fig. 7 Velocity field in the infinitely narrow crack

COMPUTATIONAL RESULTS AND DISCUSSION

Figure 8 shows the velocity fields of a unit cell (the *L/A* is 3) when *Re* number is 100 (CWL9.6A3.2), it is found that the flow malditribution is serious even *Re* number is very low when the value of *L/A* is small.

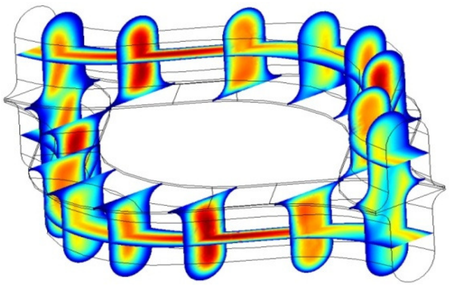

Fig. 8 Velocity field in the CW unit cell (CWL9.6A3.2)

In the CW unit cells, for the gas flows change the flow directions, there are secondary flows (shown in Fig. 9 and Fig. 10). From the velocity field it is easy to find that the velocity boundary layers are thinner near the wall when the gas flows change the flow directions. The secondary flows are the main reason for thinning the velocity boundary layers and enhancing the local heat transfer coefficient.

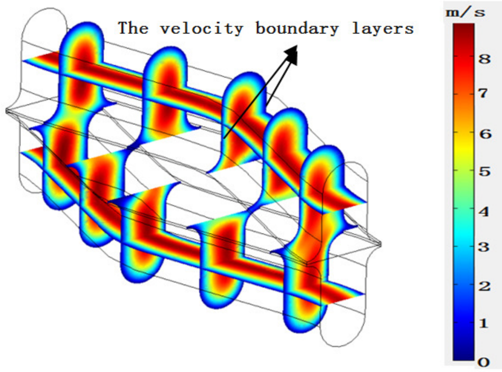

Fig. 9 Flow field in the passage with multi-boundary conditions (*Re*=100)

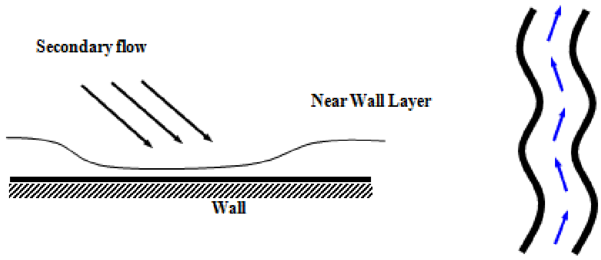

Fig. 10 Secondary flow near wall layer

Multi-periodic boundary conditions have been used in the faying surface of the unit cell, so we can use the results of the unit cell to establish the whole flow fields of the recuperator core region where the flow are fully developed. For the gas flows change flow directions in the passage, the pressure of the gas flow also change. From Fig. 11 it is found that the gas flows will go into several adjacent passages. The vorticity and the secondary flows are the main reason for the enhancement of the local heat transfer coefficient but also the increase of the pressure loss. The performance of the CW unit cell is decided by the geometrical variables and the average velocity.

The CW unit cell with different geometrical variables will have different performance. For the geometrical variables are the main parameters to influence the performance of the unit cell. In the present study, different simplified models with different wavy length and amplitude have been used to optimize the geometrical variables of the unit cell in the main flow direction.

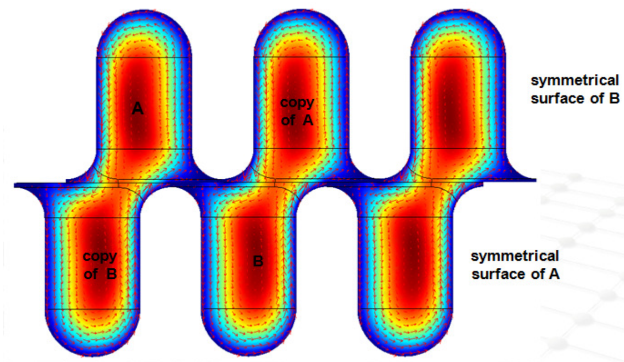

Fig. 11 Flow fields and vorticity of the cross section (*Re*=100)

Figure 12 and Fig. 13 are the flow fields in the same passage with different *Re* number. The flow maldistribution and vorticity in the passages become more serious when the *Re* number increase. When the *Re* number is big enough, there are reflux in the passages. As the *Re* number is 1000, the recirculation zone is very obvious, and the reflux will decrease the heat transfer performance and increase the pressure drop. That's why the design situation of the recuperator will be in a lower *Re* number.

Figures 14 and 15 are the flow fields in different passages with the same *Re* number. When the amplitude of the passage is bigger the malditribution and the reflux in the passages are much more serious also. The flow fields are much more complex in the unit with a smaller *L/A*, when the *A* (amplitude of the unit cell) gets bigger, the passage will open up the passage to several adjacent channels and create much larger scale secondary flows in the passages.

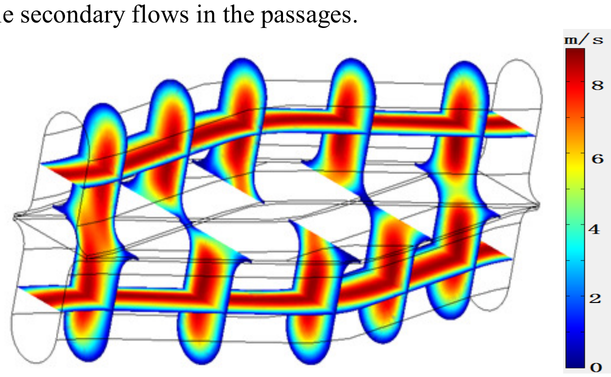

Fig. 12 Flow field in the unit cell (CWL9.6A1.2 *Re*=100)

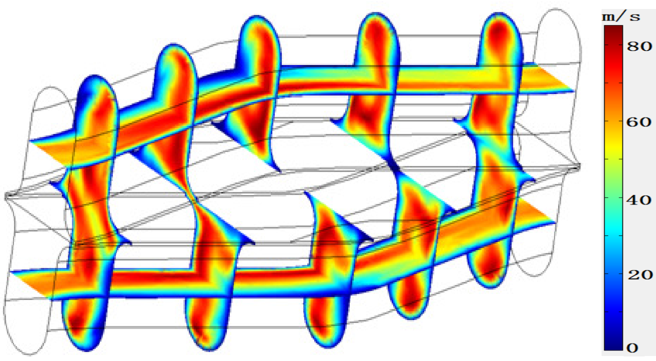

Fig. 13 Flow field in the unit cell (CWL9.6A1.2 *Re*=1000)

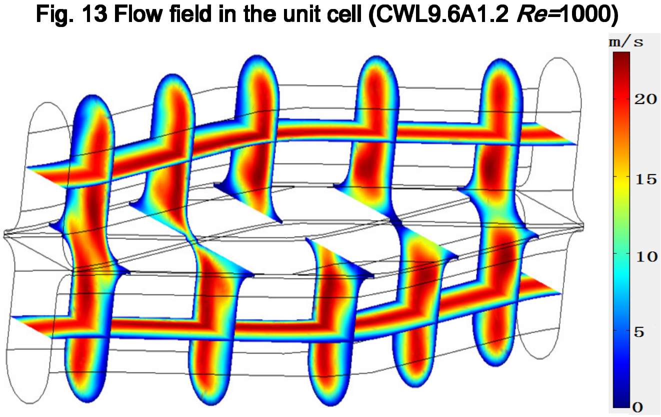

Fig. 14 Flow field in the unit cell (CWL9.6A1.2 *Re*=300)

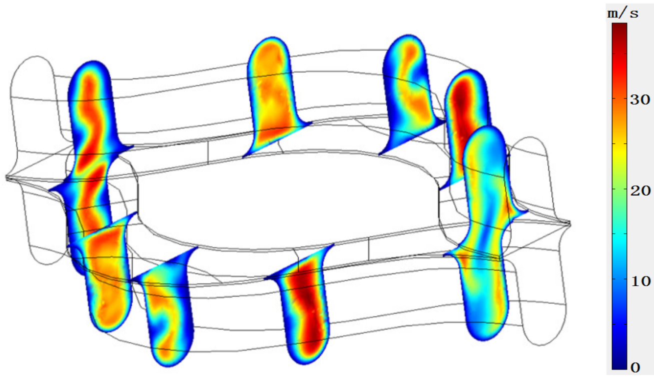

Fig. 15 Flow field in the unit cell (CWL9.6A3.2 *Re*=300)

The results of *Nu* vs. *Re* are shown in Fig. 16, the *Nu* number increases as the *Re* number increase. The passages with lower *L/A* have bigger *Nu* numbers while the *Re* numbers are the same. And when the *L/A* are the same, the passage with a shorter wavy length have higher *Nu* numbers. As the increase of *Re* and the amplitude of the channels, the secondary flows are more serious, so it is reasonable for the increase of the *Nu* and the passages with lower *L/A* have bigger *Nu* numbers.

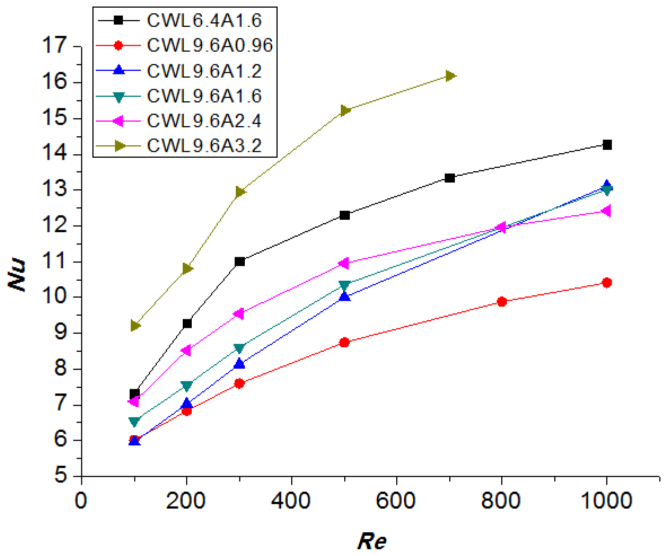

Fig. 16 *Nu* vs. *Re*

Figure 17 shows the heat transfer factor *j* vs. *Re*. The value of *j* decreases as the *Re* number increases. For the models with a lower *L/A* have a better heat transfer performance, the value of *j* is also higher. Because of the reflux and the flow maldistribution are more serious as the *Re* increase, the heat transfer factor *j* decreases.

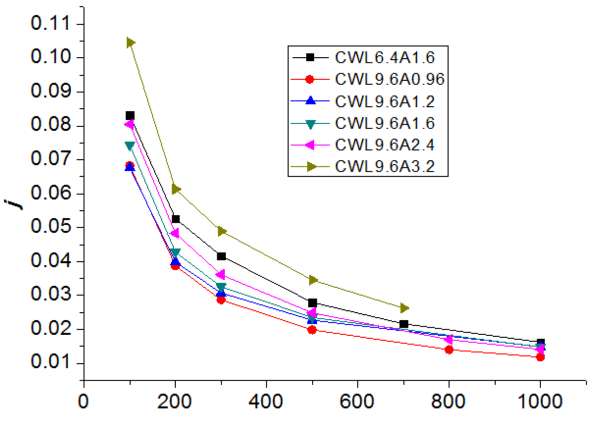

Fig. 17 *j* vs. *Re*

In Fig. 18 the friction factor for different models are plotted as a function of *Re* number. It is found that the friction factor *f* decrease quickly when the *Re* number is less than 500 and then the friction factor *f* decrease slightly as the *Re* number increase. For the hydraulic diameter of the passages is 1.689 mm, the flow in the CW unit may be into the transition state in a lower *Re* number.

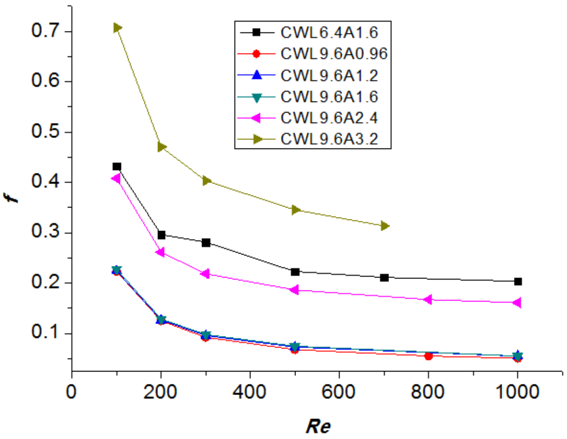

Fig. 18 *f* vs. *Re*

Figure 19 shows the performance of the CW passages. For the *Re* number is about 300 which is close to the design situation of the recuperator, the passage (CWL9.6A1.6) with *L/A* is 6 has the best performance among the models. In three cases the *j/f* increase slightly when the *Re* number is small. That means in a lower *Re* numbers, the flow maldistribution, vorticity and secondary flows enhance the general performance of the CW channels. When the *L/A* gets bigger and the *Re* number gets bigger, there is reflux in the passages which increase the pressure loss rapidly. So it is reasonable for the general performance of the unit cell decrease when *L/A* is small and the *Re* number is bigger. The cases (CWL6.4A1.6 and CWL9.6A2.4) have the same *L/A*, the case with a bigger *L* has a better performance. The length of the unit cell can reduce the reflux in the passage while the amplitude of the unit cell can create a larger scale of secondary flows and vorticity which enhance the local heat transfer coefficient. The numerical results have shown that the channel have a best performance when *L/A* is 6 among all the cases.

It is found that the amplitude and the length of the unit cell have a significant influence on the performance of the unit cell.

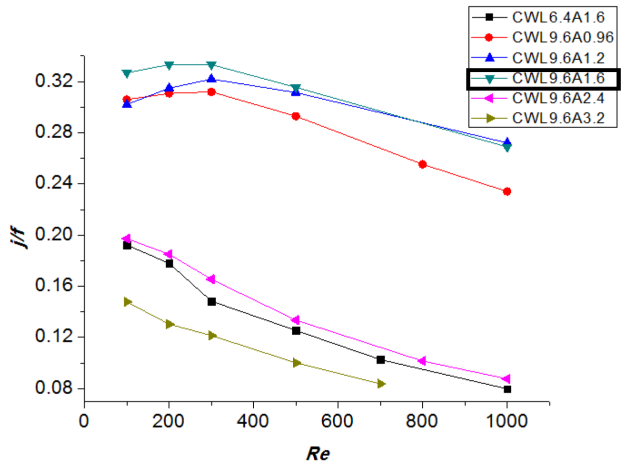

Fig. 19 *j/f* vs. Re

CONCLUSIONS

1) The simplified model with multi-periodic boundary conditions is valid to solve the flow and the heat transfer characteristic in the CW passages.
2) The amplitude of the unit cell and the length of the cell have a significant influence on the flow and the heat transfer characteristic.
3) The secondary flows and the vorticity in the passages are the main reason for the enhancement of heat transfer.
4) When the *L/A* is 6, the CW cell has the best performance among all the cases (the *Re* number is about 300). For the *L/A* is small, the flow maldistribution and the reflux are serious which increase the pressure rapidly. And the cell with large amplitude can create a large scale of secondary flows between several adjacent channels which enhance the local heat transfer coefficient.
5) The reflux and the flow malditribution in the channels are serious even in a low Re number when *L/A* is small, which decrease the general performance of the channels.

Acknowledgments

This work is supported by the National High Technology R&D Project of China (No.2008AA050501) and the Fundamental Research Funds for the Central Universities.

REFERENCES

1 McDonald C.F., Wilson D.G., The utilization of recuperated and regenerated engine cycles for high efficiency gas turbines in the 21st century [J], Journal of Applied Thermal Energy.1996,16(8/9):635-653.

2 McDonald C.F., Heat recovery exchanger technology for very small gas turbines [J], Int. Journal of Turbo and Jet Engines, 1996,13(4):239-261.
3 McDonald C.F., Low-cost compact primary surface recuperator concept for microturbines [J], Applied Thermal Engineering. 2000(20):471-497.
4 McDonald C.F., Recuperator considerations for future higher efficiency microturbines [J], Applied Thermal Engineering. 2003(23):1463-1487
5 June Kee Min, Ji Hwan Jeong , Man Yeong Ha, Kui Soon Kim, High temperature heat exchanger studies for applications to gas turbines [J], Heat Mass Transfer (2009) 46:175–186.
6 http://www.rekuperator.com/
7 Gunnar Lagerstrom, M.Sc and Max Xie, High performance &cost effective recuperator for micro-gas turbine [C], ASME TURBO EXPO, Amsterdam, 2002 3-6 June 2002.
8 Utriainen E., Sunden B., Numerical Analysis of a Primary Surface Trapezoidal Cross Wavy Duct [J], International Journal of Numerical Methods for Heat & Fluid Flow, 2000, 10:634-648.
9 Utriainen E. and Sundén B., A numerical investigation of primary surface rounded cross wavy ducts [J], Heat and Mass Transfer ,2002, 38(7-8):537-542.
10 Lagerstrom G, Xie M (2002) High performance and cost effective recuperator for micro-gas turbines [J], ASME Turbo Expo, Amsterdam, GT-2002-30402.
11 Stasiek JA, Experimental studies of heat transfer and fluid flow across corrugated-undulated heat exchanger surfaces [J], Heat Mass Transfer 1998 41(6/7):899–914.
12 Q.W. Wang, L.Q. Luo, H.X. Liang, J.W. Wang, Z.P. Huang, Z.P. Feng and Z.Q. Chen, Experimental Investigation on Heat Transfer and Pressure Drop in a Microtubine Recuperator with Cross-Wavy Primary Surface Channels [C], ASME Turbo Expo 2005, Reno Hilton, Reno-Tahoe, Nevada, USA, June 6-9, 2005.
13 Mario L. Ferrari et al, Micro Gas Turbine Recuperator: Steady-State and Transient Experimental Investigation [J], Journal of Engineering for Gas Turbines and Power FEBRURY 2010, vol. 132/022301-1.
14 M. Ciofalo, Investigation of flow and heat transfer in corrugated passages-II Numerical simulations [J], Heat Mass Transfer, 1996, vol.39, No.1/165-192.
15 W.Q. Tao, Numerical Heat Transfer [M], Xi'an jiaotong university Press..2002, 489-491.

